

Kinetic studies of direct blue photodegradation over flower-like TiO₂

Han Zhang¹ · Delei Liu¹ · Shan Ren¹ · Hui Zhang^{1,2}

Received: 7 June 2016 / Accepted: 27 August 2016 / Published online: 26 September 2016
© Springer Science+Business Media Dordrecht 2016

Abstract The kinetics of photocatalytic oxidation reaction for direct blue solution was studied by using flower-like TiO₂ under the irradiation of ultraviolet (UV) light. A series of possible affecting factors were studied, including pH value, the additive amount of light catalyst, H₂O₂ and with or without Ag modification. The kinetics of photocatalytic degradation under UV was found following a pseudo-second-order reaction kinetic model with high regression coefficients (R^2). It has been demonstrated that the initial concentration and its related factors have influenced the photocatalytic degradation efficiency and corresponding kinetic parameters. Also, the kinetic parameter k is increasing with the degradation efficiency.

Keywords Flower-like TiO₂ · Photocatalytic · Reaction kinetics

Introduction

Recently, the treatment of dye wastewater has been one of the most active fields in heterogeneous photocatalysis. This provokes a potential value based on titanium dioxide (TiO₂) for gas and water treatment applications. Generally, the entire process of photocatalytic reaction occurs mainly on the surface of TiO₂ [1–3]. Photocatalytic reaction efficiency has a close relation with active sites, which decides the nature of the photocatalyst and related operating conditions [4, 5].

✉ Hui Zhang
huizhang@swpu.edu.cn; zhanghuiswpu@126.com

¹ College of Chemistry and Chemical Engineering, Southwest Petroleum University, Chengdu 610500, China

² Oil and Gas Field Applied Chemistry Key Laboratory of Sichuan Province, Chengdu 610500, China

As a semiconductor, TiO_2 exhibits specific properties for organics degradation due to its high photo-activity, which has attracted considerable attention [6–8]. These characteristics, like morphology, surface area, crystalline phase composition and surface hydroxyl concentration, were considered as the main affecting factors of photocatalytic activity. Meanwhile, the operating conditions of the system also greatly affect the photocatalytic activity. Generally, TiO_2 photocatalysts were evaluated for catalytic degradation of organics, and most of them exhibited excellent catalytic performance on different pollutants and degradation conditions [9–11]. The photodegradation of direct blue (DB) over flower-like TiO_2 was studied in this work.

There are many studies on wastewater decomposition with TiO_2/UV , which investigate a number of factors that could influence the photocatalysis efficiency and make use of the kinetic model to explain their results. Priya and Madras [12] investigated the photocatalytic reaction process for the degradation of chlorophenol and nitrophenol on synthesized nano- TiO_2 . They also proposed a modified Langmuir–Hinshelwood kinetic model, as well as obtained correlative kinetic parameters in accordance with the initial rate analysis. Smith et al. [13] examined the effect of the physicochemical parameters of methyl orange degradation, and concluded a simple correlation between photo-electrochemical properties, light intensity, and dye concentration base on a Langmuir–Hinshelwood mechanism. Basha et al. [14] integrated photo-catalytic adsorbents and photo-degradation of indomethacin in aqueous solutions based on TiO_2 -activated carbon. It was found that the kinetics of photocatalytic degradation follow a Langmuir–Hinshelwood model. By analyzing and comparing the adsorption rate constant and light catalytic rate constant, it was concluded that the photocatalysis of indomethacin is a rate-determining step in the process of adsorption and photocatalysis. However, most of the reports explain their experimental results by just adopting the same model and method without considering the limitations of the model, and the detailed reaction mechanism. Generally, the application of a Langmuir–Hinshelwood model is built on ideal assumptions, which include the reaction system being in dynamic equilibrium; the reaction is surface-mediated; and the competition for the TiO_2 active surface sites by the intermediates and other reactive oxygen species is not limited [15, 16]. It is inappropriate that the detailed reaction mechanism of photocatalytic degradation of DB remains to be further explored. According to available reports, we found that simpler zero, first- or second-order kinetics are sufficient to simulate the process of photocatalytic reaction of organic compounds [5, 17]. These simple kinetic models of the photocatalytic reaction presented were not limited to the use of a Langmuir–Hinshelwood model, and can accommodate any rate law expression. Thus, these simple models can be used to describe the photo-degradation process of DB. This study presents systematic research, including pH value, the additive amount of light catalyst, H_2O_2 and with or without Ag modification. The study of photocatalytic oxidation kinetics helps to understand the reaction mechanism, control the reaction trend and discern the optimum operating conditions of DB photocatalytic degradation; parameters obtained also provide the requisite conditions for the design of efficient photocatalysts and optimization of the reaction conditions.

Experimental

Catalyst preparation

All reagents used in this work were of analytical grade. Combined with the previously reported methods [18–22], the flower-like TiO₂ was prepared by the hydrothermal method. As is common in methods of preparation experiments, 0.005 mol titanium isopropoxide was added to a mixture of 20 mL of glycerol and 20 mL of isopropanol. There was a 10-min mixing process at room temperature before the suspension was transferred to a 100-mL Teflon-lined autoclave. The autoclave was maintained at 180 °C under autogeneous pressure for 16 h. After cooling, the white product could be obtained after filtrating and washing with water and ethanol. Then, the solid product was dried at 60 °C for 24 h, followed by calcination at 450 °C in air for 2 h.

Characterization

The X-ray diffraction (XRD) spectra were examined on an X'Pert PRO MPD diffractometer with Cu-K α radiation ($\lambda = 0.154056$ nm, 30 kV, 30 mA).

The morphology of the sample was observed via scanning electron microscopy (SEM) using a JEOL/EO JSM-5900. A JEOL-JEM-2011 instrument with an accelerating voltage of 200 kV was also used. The structures of the samples were analyzed by high-resolution transmission electron microscopy (HRTEM) using an FEI Tecnai G20 apparatus operating at 200 kV.

N₂ adsorption–desorption isotherms were measured at 77 K using a Quadrasorb evoTM (Quantachrome Company, FL, USA). Prior to measurements, the TiO₂ powders were degassed under a primary vacuum at 150 °C for 3 h using a FloVac ST-MP-9 instrument. Brunauer–Emmett–Teller (BET) methods were applied to determine the specific area. The pore size distribution and the average pore size were determined using the Barret–Joyner–Halenda (BJH) model.

Photo-catalytic performance evaluation

According to the references reported in publications [23–25], photocatalytic activities were measured in a home-made photo-reactor. The reactor is completely opaque, with ultraviolet light with wavelength of 320–400 nm. During the whole experiment, the experimental conditions were controlled at room temperature (298 K) and atmospheric pressure (101.325 kPa). The experiment process can be expressed as below: TiO₂ catalysts were dispersed in homogenous DB solution (100 mL) with the help of ultrasonic. To attain adsorption–desorption equilibrium, the suspension was stirred with bubbling air in the dark for 30 min. At certain time intervals, 5 mL of the mixed suspensions were collected, centrifuged via high-speed centrifugation and measured by a Hitachi F-4500 FL spectrophotometer. The dye concentration can be calculated according to the Beer–Lambert curves to correlate the absorbance at its characteristic absorption wavelengths (598 nm).

Results and discussion

Characterization of TiO₂ microspheres

The crystal structure of flower-like TiO₂ was detected by X-ray diffraction (XRD) measurements. Figure 1 displays diffraction peaks of the sample which are in agreement with the previous publication. The average size of TiO₂ was about 16 nm (Table 1) which was calculated from the most intense XRD peak (101) by using Scherrer's formula. Earlier work suggests that this crystallization size could be related to the concentration of titanium oxide crystallization sites during the hydrolysis of tetrabutyl titanate [26].

The SEM and TEM images of microspheres are presented in Fig. 2. A daisy-like morphology and uniform microspheres with the size of ~1 μm were detected by SEM and TEM. The flower-like TiO₂ is composed of many thin TiO₂ nanobelts with a stab on the top displayed in Fig. 2a, b. The TEM image (Fig. 2c) reveals the size of the TiO₂ nanobelts ranges 20–50 nm, and its thickness is around 6 nm. The lattice fringes in the HRTEM image (Fig. 2d) give interplanar distances of 0.35 and 0.48 nm corresponding to the (101) planes and the (010) planes, respectively. The selected area electron diffraction (SAED) pattern inset in Fig. 2c confirmed preferential exposure faces of (101) planes and (010) planes over synthesized flower-like nanoparticles [27].

The specific surface area and porosity of the as-synthesized samples were investigated by using nitrogen adsorption and desorption isotherms. As shown in Fig. 3, the isotherm of flower-like TiO₂ is identified as type IV with a H₃ hysteresis loop, which suggests its mesoporous feature [28]. Also, the corresponding pore size distribution curves calculated using the BJH method were shown in Fig. 3. The specific surface area, total pore volume and average pore diameter are displayed in Table 1.

Fig. 1 XRD patterns of flower-like TiO₂ nanoparticles

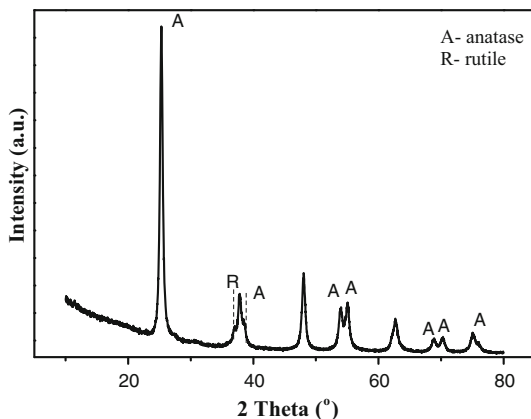
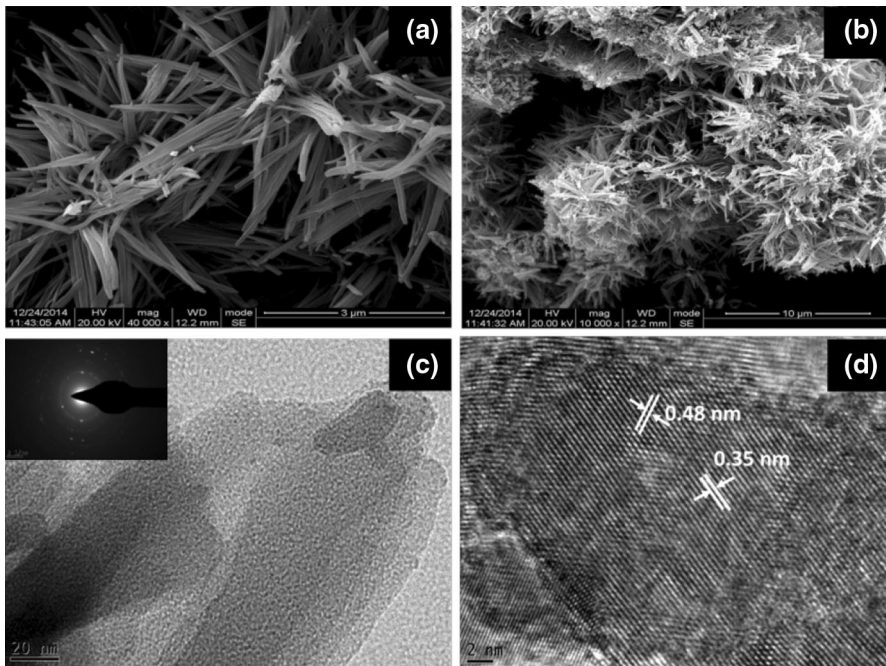


Table 1 Textural properties of flower-like TiO₂

Catalysts	S _{BET} (m ² /g)	Pore volume (cm ³ /g)	Average pore diameter (nm)	Crystallization size ^a (nm), XRD
Flower-like TiO ₂	41.59	0.2089	3.678	15.80

^a BJH method**Fig. 2** SEM (a, b) and TEM (c, d) images for flower-like TiO₂

Optimizing interference factors

Mechanism

Since the photo-generated carriers can induce oxidation and reduction processes, the titanium dioxide is widely used as a photocatalyst [29]. According to the extensive literature, when aqueous solution was irradiated in the presence of TiO₂ photocatalyst, the adsorbed water molecules reacted with the holes in the valence band to form hydroxyl radicals and release hydrogen ions. The hydroxyl radical is one of the most powerful oxidants. It can initiate multiple oxidation reactions, which leads to the complete mineralization of original organic matter and its degradation products [30, 31, 33].

According to many reports, the reaction of hydroxyl radicals with organic matter can be summarized as a dehydrogenation process [30, 32].

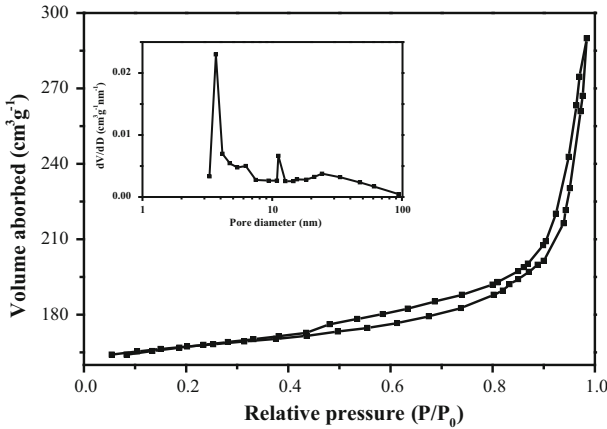
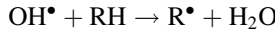


Fig. 3 Nitrogen adsorption–desorption isotherms and the corresponding pore size distributions curve (*inset*) of flower-like TiO₂



For quantitative evaluation, the zero-order, first-order, and second-order kinetics equations were fitted to the experimental data. These models are given by the following equations [34]:

$$r = -\frac{dC}{dt} = k_{\text{photo},0}$$

$$r = -\frac{dC}{dt} = k_{\text{photo},1}C$$

$$r = -\frac{dC}{dt} = k_{\text{photo},2}C^2$$

where r is the rate of DB concentration ($\text{mmol L}^{-1} \text{min}^{-1}$), C is the concentration at any time (mmol L^{-1}), $k_{\text{photo},0}$ is the zero-order rate constant ($\text{mmol L}^{-1} \text{min}^{-1}$), $k_{\text{photo},1}$ is the first-order rate constant (min^{-1}), and $k_{\text{photo},2}$ is the second-order rate constant ($\text{L mmol}^{-1} \text{min}^{-1}$).

The non-linearized forms of the zero-order, first-order, and second-order kinetics expressions are obtained as follows:

$$C = C_0 - k_{\text{photo},0}t$$

$$C = C_0 \exp^{-k_{\text{photo},1}t}$$

$$C = \frac{C_0}{1 + k_{\text{photo},2}tC_0}$$

where C_0 is the initial concentration of the solution. Nonlinear regression was used to estimate the parameters involved in the zero-order, first-order, and second-order kinetics expressions.

Select the dynamic equations

The time-concentration curves (Fig. 4.) obtained from the oxidation experiments of DB and each individual initial concentration were fitted to a potential kinetic equation.

As shown in Table 2, regression coefficients (R^2) were low based on the zero-order and first-order kinetics, and ranged from 0.2116 to 0.8407 and 0.8238 to 0.9095, respectively, confirming the unsatisfactory fit of the experimental data for TiO_2 photocatalysis to the zero-order and first-order model.

While the second-order kinetics expression exhibited an improved fit, the again-improved R^2 for the second-order kinetics model shows that it best represents the kinetics of DB degradation by TiO_2 . According to pseudo-second-order reaction parameters (Table 2), the reaction rate constant decreases with increasing initial concentration, when the DB solution is at a lower concentration (0.05–0.15 mmol L^{-1}). It can be explained as follows: The essence of photocatalytic reaction is the indirect photolysis reaction of hydroxyl radicals ($\text{OH}\cdot$) and organic compounds. As the concentration of dye increases, less H_2O molecules are adsorbed on the catalyst surface. The number of hydroxyl radicals formed on the catalyst surface is strictly restricted. Hence, the photocatalysis kinetic parameters of DB on flower-like TiO_2 were greatly reduced with an increase of dye concentration [35, 36].

The influence of pH value on light catalytic properties

The effect of pH of solution on the decolorization of DB dye is depicted in Fig. 5. Also, the relevant second-order kinetic parameters are listed in Table 3. It can be seen that the removal percentage of DB and the second-order kinetics parameters increased as the pH decreasing. Clearly, the second-order kinetics provide a good fit

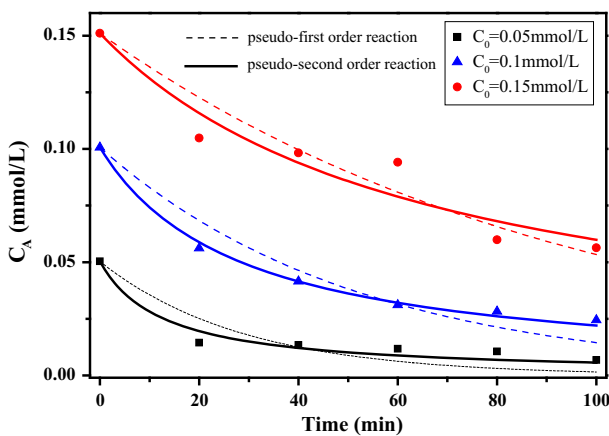
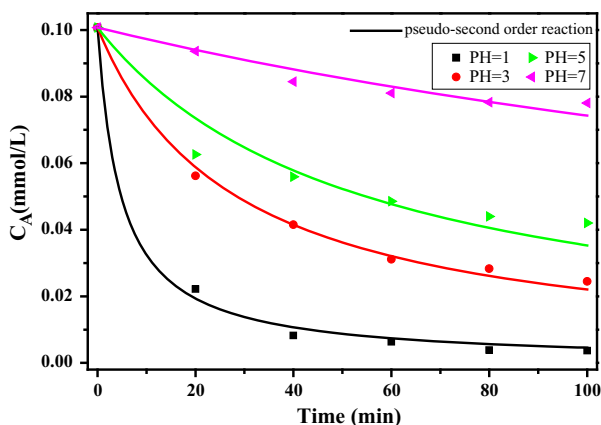


Fig. 4 Different initial concentrations of the DB solution on the dye removal (100 mL of DB solution, pH 3.0, 30 mg/L photocatalysis) plots based on first-order, and second-order kinetics fitted to the experimental data for UV illumination, respectively

Table 2 Photocatalysis kinetic parameters of DB on flower-like TiO₂ nanoparticles at different initial concentration with the kinetic model

Kinetic model	Kinetic parameters	C ₀ (mmol L ⁻¹)		
		0.05	0.1	0.15
Zero-order reaction				
$C = C_0 - k_{\text{photo},0}t$	$k_{\text{photo},0}$ (mmol L ⁻¹ min ⁻¹)	0.000547	0.0009479	0.001055
	R ²	0.2116	0.6052	0.8407
Pseudo-first-order reaction				
$C = C_0 \exp^{-k_{\text{photo},1}t}$	$k_{\text{photo},1}$ (min ⁻¹)	0.03472	0.01937	0.0104
	R ²	0.8238	0.9255	0.9095
Pseudo-second-order reaction				
$C = \frac{C_0}{1+k_{\text{photo},2}tC_0}$	$k_{\text{photo},2}$ (L mmol ⁻¹ min ⁻¹)	1.56	0.354	0.1008
	R ²	0.9602	0.9956	0.9245

**Fig. 5** DB solution with different pH on the surface of flower-like TiO₂ removal (0.1 mmol L⁻¹ initial concentration, 100 mL DB solution, 30 mg/L photocatalysis) plots based on second-order kinetics fitted to the experimental data

to the experimental data for TiO₂ photocatalysis as regression coefficients (Table 3) were greater than 0.9 and ranged from 0.9249 to 0.9974.

In a heterogeneous photocatalytic system, pH is an important operating parameter. The charge on the catalyst particles, size of catalyst aggregates and valence bands are affected by pH. Thus, the photocatalytic activities would vary with the pH values [5]. By changing the pH values of the solution, the protonated or deprotonated reaction can be realized on the surface of TiO₂. According to the acidic or alkaline conditions, the reaction equation can be expressed as follow [37, 38]:

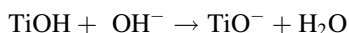
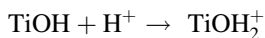


Table 3 The second-order kinetic parameters of photocatalytic degradation of DB with different pH

Kinetic parameters	pH			
	1	3	5	7
$k_{\text{photo},2}$ (L mmol ⁻¹ min ⁻¹)	2.088	0.3541	0.184	0.03533
R^2	0.9974	0.9956	0.9249	0.9251

For the photocatalytic reactions on the surface of TiO₂, pH values of the system have been extensively studied. It is reported that TiO₂ has a higher oxidizing activity in acidic solution [37, 39], but the production rate of hydroxyl radicals can decrease with excess H⁺. But, excess H⁺ at low pH can decrease the reaction rate. According to the reports of Shifu and Gengyu [40], we found that the photo-generated holes (h⁺) are the predominant oxidizing species at low pH. However, it should also be noticed that hydroxyl radicals are rapidly scavenged at high pH due to the abundance of hydroxyl ions which inhibits its reaction to some extent [41]. Therefore, within a certain range of pH values, enhancement of pH is beneficial to photocatalytic degradation of DB in the presence of TiO₂.

The influence of the additive amount of light catalyst

As shown in Fig. 6, a series of DB decomposition tests were carried out with TiO₂ solid content being varied from 0 to 75 mg/L. Clearly, the DB decomposition rate seems to increase with the TiO₂ concentration (<60 mg/L) and then slightly decreases with the TiO₂ concentration (>60 mg/L). The second-order kinetics model is also used to fit the experimental data, and relevant parameters are shown in Table 4. The second-order kinetic parameters increase with the DB decomposition rate, and up to 3.004 L mmol⁻¹ min⁻¹ at 60 mg/L TiO₂ photocatalysis.

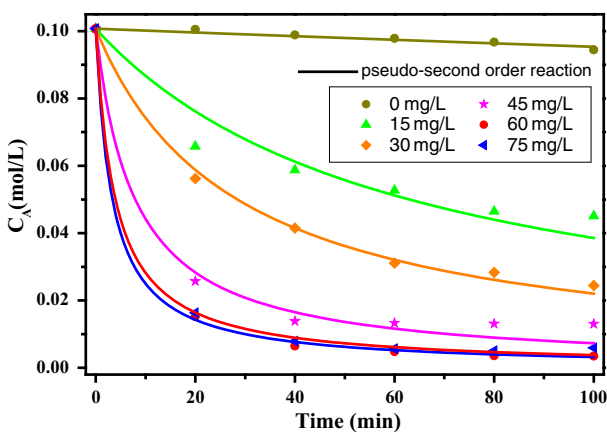


Fig. 6 Flower-like TiO₂ with different concentrations for DB removal (0.1 mmol L⁻¹ initial concentration, 100 mL DB solution, pH 3.0) plots based on second-order kinetics fitted to the experimental data

Table 4 The second-order kinetic parameters of photocatalytic degradation of DB with different dosage of photocatalysts

Kinetic parameters	C_{TiO_2} (mg/L)					
	0	15	30	45	60	75
$k_{\text{photo},2}$ (L mmol ⁻¹ min ⁻¹)	0.005597	0.16	0.3541	1.268	3.004	2.548
R^2	0.9243	0.9229	0.9956	0.9891	0.9996	0.9992

In a heterogeneous photocatalytic treatment system, the concentration of TiO₂ is one of the most important factors for the overall reaction rate [37]. The effectiveness of active sites on the TiO₂ surface, as well as the availability of photo-activating light penetration in the suspension, all can be used to illustrate the effect of catalyst concentration. The quantity of the active sites increases with the catalyst concentration in the suspension, but the light penetration decreases with the catalyst concentration in the suspension due to the screening effect [42, 43]. In order to avoid excess catalyst and ensure total absorption of efficient photons, 60 mg/L TiO₂ photocatalysis is considered as the best condition for photocatalytic degradation of DB.

The influence of H₂O₂

As showed in Fig. 7, a series of experiments with variations of H₂O₂ was performed. It was observed that the TiO₂ together with H₂O₂ had a beneficial effect on the degradation of the DB dyes. The DB decomposition rate increases with the addition of H₂O₂ (<5 ml/L) and then remained at a similar rate. This fact could be attributed to a more efficient generation of hydroxyl radicals and inhibition of electron–hole pair recombination from the right amount of H₂O₂. The second-order

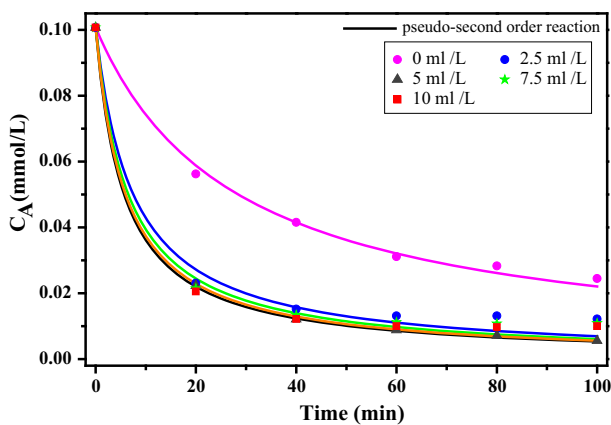


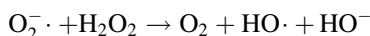
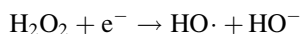
Fig. 7 DB solution with variations of H₂O₂ on the surface of flower-like TiO₂ removal (0.1 mmol L⁻¹ initial concentration, 100 mL DB solution, pH 3.0, 30 mg/L photocatalysis) plots based on second-order kinetics fitted to the experimental data

Table 5 The second-order kinetic parameters in DB's photocatalytic degradation with variation of H₂O₂

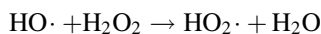
Kinetic parameters	V ml (H ₂ O ₂)/L _(DB solution)				
	0	2.5	5.0	7.5	10
$k_{\text{photo},2}$ (L mmol ⁻¹ min ⁻¹)	0.3541	1.341	1.742	1.546	1.686
R^2	0.9956	0.9885	0.9999	0.9929	0.9948

kinetics model is also used to fit the experimental data, and the relevant parameters are shown in Table 5. It can be seen that the second-order kinetic parameters increased with the DB decomposition rate, and up to 1.774 L mmol⁻¹ min⁻¹ with the addition of 5 ml/L H₂O₂.

Currently, many researchers have reported the addition of H₂O₂ in enhancing TiO₂ photocatalysis reactions, although H₂O₂ may be generated via the TiO₂ photocatalysis [44, 45]. The H₂O₂ can inhibit the recombination of electron-hole pairs, and further provides additional OH· radicals through the following mechanisms [5, 46]:



Further, addition of H₂O₂ was found to decrease the overall reaction rate in several studies, owing to the formation of less penetrative HO₂· radicals, as described by



Thus, for comparison purposes, the optimal amount of H₂O₂ (5 ml/L) is selected in this study.

The influence of Ag modification

As is shown in Fig. 8, the rate of photocatalytic reaction is strongly influenced by the photocatalyst. Photocatalyst modification plays a vital role in the improvement of photocatalysis efficiency. Heterogeneous photocatalytic reactions are known to show a dramatic increase in photo-degradation with catalyst loading. The second-order kinetics model for the degradation of DB is also used to fit the experimental data, and relevant parameters are shown in Table 6. Also, the reaction rate constant increases with the efficiency of the photocatalytic reaction.

Doping low-concentration silver ions on the TiO₂ surface, migration and diffusion of Ag ions are dominant in the process of photocatalysis. AgO as well as Ag₂O are the major chemical states of Ag ions. Thus, the recombination of electron-hole pairs can be effectively inhibited. Furthermore, compared to pure TiO₂, the content of adsorbed O₂ and surface hydroxyls on the surface of Ag-TiO₂ increased significantly with the photoinduction. This can be used to explain the fact

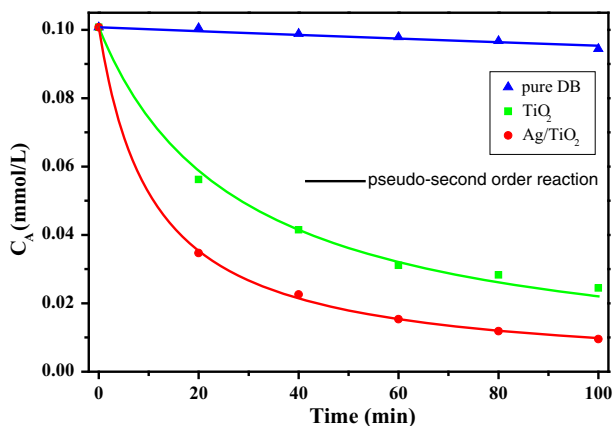


Fig. 8 Plots of DB dye removal on the surface of 0.5 % Ag/TiO₂ (0.1 mmol L⁻¹ initial concentration, 100 mL DB solution, pH 3.0, 30 mg/L photocatalysis) based on second-order kinetics fitted to the experimental data

Table 6 The second-order kinetic parameters of photocatalytic degradation of DB with Ag modification

Kinetic parameters	Pure DB	30 mg/L TiO ₂	30 mg/L Ag/TiO ₂
$k_{\text{photo},2}$ (L mmol ⁻¹ min ⁻¹)	0.005597	0.3541	0.9179
R^2	0.9243	0.9956	0.9997

that a small amount of Ag ions can significantly improve the efficiency of photocatalytic degradation DB [47, 48].

Conclusions

Flower-like TiO₂ was prepared by a hydrothermal method and its photocatalytic activities were evaluated by using direct blue as a probe molecule. It was also found to be an active photocatalyst in photo-decolorization of DB dye under UV irradiation, owing to its unique particle morphological structure.

Reaction kinetics studies suggests that the experimental data follow the pseudo-second-order reaction model, as regression coefficients all were greater than 0.9. The second-order kinetic parameters of photocatalytic degradation of DB were successfully used to study the effect of dye concentration, pH value, the additive amount of light catalyst, H₂O₂ and with or without Ag modification, which indicate that there is a close relationship between the photocatalytic activity and second-order kinetic parameters. According to the results, the second-order kinetic parameter k is increasing with the photocatalytic activity. Therefore, when investigating an operation factor, a larger k is better for the DB's photocatalytic degradation under the same conditions.

Acknowledgments This work was supported by the National Natural Science Foundation of China (NSFC-21406184) and Scientific Research Starting Project of SWPU (No. 2014QHZ013). The authors would like to thank Peng Shi, Fei Huang and Pengfei Zhu for their useful discussions and help.

References

1. X. Rong, F. Qiu, C. Zhang, L. Fu, Y. Wang, D. Yang, *Ceram. Int.* **2502**, 41 (2015)
2. D. Zhang, J. Yang, S. Bao, Q. Wu, Q. Wang, *Sci. Rep.* **1399**, 3 (2013)
3. B. Qiu, Y. Zhou, Y. Ma, X. Yang, W. Sheng, M. Xing, J. Zhang, *Sci. Rep.* **8591**, 5 (2015)
4. G. Tian, Y. Chen, W. Zhou, K. Pan, C. Tian, X. Huang, H. Fu, *CrystEngComm* **2994**, 13 (2011)
5. M.N. Chong, B. Jin, C.W.K. Chow, C. Saint, *Water Res.* **2997**, 44 (2010)
6. G. Liu, H.G. Yang, J. Pan, Y.Q. Yang, G.Q.M. Lu, H. Cheng, *Chem. Rev.* **9559**, 114 (2014)
7. Y. Ma, X. Wang, Y. Jia, X. Chen, H. Han, C. Li, *Chem. Rev.* **9987**, 114 (2014)
8. W. Wang, C. Lu, Y. Ni, M. Su, Z. Xu, *Mater. Lett.* **11**, 79 (2012)
9. T.A. Westrich, K.A. Dahlberg, M. Kaviani, J.W. Schwank, *J. Phys. Chem. C* **16537**, 115 (2011)
10. R. Su, M. Christensen, Y. Shen, J. Kibsgaard, B. Elgh, R.T. Vang, R. Bechstein, S. Wendt, A. Palmqvist, B.B. Iversen, F. Besenbacher, *J. Phys. Chem. C* **27039**, 117 (2013)
11. W. Li, Z. Wu, J. Wang, A.A. Elzatahry, D. Zhao, *Chem. Mater.* **287**, 26 (2014)
12. M.H. Priya, G. Madras, *Ind. Eng. Chem. Res.* **482**, 45 (2006)
13. Y.R. Smith, A. Kar, V.R. Subramanian, *Ind. Eng. Chem. Res.* **10268**, 48 (2009)
14. S. Basha, D. Keane, A. Morrissey, K. Nolan, M. Oelgemöller, J. Tobin, *Ind. Eng. Chem. Res.* **11302**, 49 (2010)
15. C. Minero, *Catal. Today* **205**, 54 (1999)
16. C.P.E.M. Minero, *Sol. Energy* **421**, 56 (1996)
17. I. Salvadó-Estivill, D.M. Hargreaves, G. Li Puma, *Environ. Sci. Technol.* **2028**, 41 (2007)
18. Z. Sun, J.H. Kim, Y. Zhao, F. Bijarbooneh, V. Malgras, Y. Lee, Y. Kang, S.X. Dou, *J. Am. Chem. Soc.* **19314**, 133 (2011)
19. L. Mao, Y. Wang, Y. Zhong, J. Ning, Y. Hu, *J. Mater. Chem. A* **8101**, 1 (2013)
20. T. Zhu, J. Li, Q. Wu, A.C.S. *Appl. Mater. Interfaces* **3448**, 3 (2011)
21. C. Wang, L. Yin, L. Zhang, Y. Qi, N. Lun, N. Liu, *Langmuir* **12841**, 26 (2010)
22. A.K. Sinha, S. Jana, S. Pande, S. Sarkar, M. Pradhan, M. Basu, S. Saha, A. Pal, T. Pal, *CrystEngComm* **1210**, 11 (2009)
23. R. Su, R. Tiruvalam, A.J. Logsdail, Q. He, C.A. Downing, M.T. Jensen, N. Dimitratos, L. Kesavan, P.P. Wells, R. Bechstein, H.H. Jensen, S. Wendt, C.R.A. Catlow, C.J. Kiely, G.J. Hutchings, F. Besenbacher, *ACS Nano* **3490**, 8 (2014)
24. S.C. Roy, O.K. Varghese, M. Paulose, C.A. Grimes, *ACS Nano* **1259**, 4 (2010)
25. D.S. Ovoshchnikov, B.G. Donoeva, V.B. Golovko, *ACS Catal.* **34**, 5 (2015)
26. E.J.W. Crossland, N. Noel, V. Sivaram, T. Leijtens, J.A. Alexander-Webber, H.J. Snaith, *Nature* **215**, 495 (2013)
27. M.C. Hidalgo, M. Maicu, J.A. Navío, G. Colón, *J. Phys. Chem. C* **12840**, 113 (2009)
28. R. Hao, X. Xiao, X. Zuo, J. Nan, W. Zhang, *J. Hazard. Mater.* **137**, 209 (2012)
29. S. Saha, J.M. Wang, A. Pal, *Sep. Purif. Technol.* **147**, 89 (2012)
30. C.G. Maia, A.S. Oliveira, E.M. Saggiaro, J.C. Moreira, *React. Kinet. Mech. Catal.* **305**, 113 (2014)
31. S.T. Martin, W. Choi, M.R. Hoffman, *Chem. Rev.* **69**, 95 (1995)
32. M. Muruganandham, M. Swaminathan, *Dyes Pigm.* **133**, 68 (2006)
33. E.M. Saggiaro, A.S. Oliveira, T. Pavesi, C.G. Maia, L.F.V. Ferreira, J.C. Moreira, *Molecules* **10370**, 16 (2011)
34. S. Basha, D. Keane, A. Morrissey, K. Nolan, M. Oelgemöller, J. Tobin, *Ind. Eng. Chem. Res.* **11302**, 49 (2010)
35. A. Hu, R. Liang, X. Zhang, S. Kurdi, D. Luong, H. Huang, P. Peng, E. Marzbanrad, K.D. Oakes, Y. Zhou, M.R. Servos, *J. Photochem. Photobiol. A* **7**, 256 (2013)
36. V. Subramanian, P.V. Kamat, E.E. Wolf, *Ind. Eng. Chem. Res.* **2131**, 42 (2003)
37. U.I. Gaya, A.H. Abdullah, *J. Photochem. Photobiol. C* **1**, 9 (2008)
38. M.N. Chong, B. Jin, C.W.K. Chow, C.P. Saint, *Chem. Eng. J.* **158**, 152 (2009)
39. J. Sun, X. Wang, J. Sun, R. Sun, S. Sun, L. Qiao, *J. Mol. Catal. A: Chem.* **241**, 260 (2006)
40. C. Shifu, C. Gengyu, *Sol. Energy* **1**, 79 (2005)

41. K.M. Lee, S.B. Abdul Hamid, C.W. Lai, *Mater. Sci. Semicond. Process.* **40**, 39 (2015)
42. C. Wu, J. Chern, *Ind. Eng. Chem. Res.* **6450**, 45 (2006)
43. S. Zhou, A.K. Ray, *Ind. Eng. Chem. Res.* **6020**, 42 (2003)
44. J.A. Zazo, J.A. Casas, A.F. Mohedano, M.A. Gilarranz, J.J. Rodríguez, *Environ. Sci. Technol.* **9295**, 39 (2005)
45. P.K. Dutta, S.O. Pehkonen, V.K. Sharma, A.K. Ray, *Environ. Sci. Technol.* **1827**, 39 (2005)
46. I.K. Konstantinou, T.A. Albanis, *Appl. Catal. B* **1**, 49 (2004)
47. B. Xin, L. Jing, Z. Ren, B. Wang, H. Fu, *J. Phys. Chem. B* **2805**, 109 (2005)
48. D. Yang, Y. Sun, Z. Tong, Y. Tian, Y. Li, Z. Jiang, *J. Phys. Chem. C* **5827**, 119 (2015)